J. Cent. South Univ. (2022) 29: 1945−1956
DOI: https://doi.org/10.1007/s11771-022-5056-z

Springer

Experimental study on mechanical properties of basalt fiber-reinforced silty clay

JIA Yu(贾羽)[1], ZHANG Jia-sheng(张家生)[1, 2], WANG Xuan(王晅)[1, 2],
DING Yu(丁瑜)[1]*, CHEN Xiao-bin(陈晓斌)[1, 2], LIU Tao(柳涛)[3]

1. Geotechnical Engineering, School of Civil Engineering, Central South University, Changsha 410083, China;
2. National Engineering Research Center of High-Speed Railway Construction Technology, Central South University, Changsha 410083, China;
3. China Railway Siyuan Survey and Design Group Co., Ltd., Wuhan 430060, China

Abstract: Fiber reinforcement technology can significantly improve the mechanical properties of soil and has been increasingly applied in geotechnical engineering. Basalt fiber is a new kind of environment-friendly and high-performance soil reinforcement material, and the mechanical properties of basalt fiber-reinforced soil have become a hot research topic. In this paper, we conducted monotonic triaxial and cyclic triaxial tests, and analyzed the influence of the fiber content, moisture content, and confining pressure on the shear characteristics, dynamic modulus, and damping ratio of basalt fiber-reinforced silty clay. The results illustrate that basalt fiber can enhance the shear strength of silty clay by increasing its cohesion. We find that the shear strength of reinforced silty clay reaches its maximum when the fiber content is approximately 0.2% and the moisture content is 18.5% (optimum moisture content). Similarly, we also find that the dynamic modulus that corresponds to the same strain first increases then decreases with increasing fiber content and moisture content and reaches its maximum when the fiber content is approximately 0.2% and the moisture content is 18.5%. The dynamic modulus is positively correlated with the confining pressure. However, the change in the damping ratio with fiber content, moisture content, and confining pressure is opposite to that of the dynamic modulus. It can be concluded that the optimum content of basalt fiber for use in silty clay is 0.2%. After our experiments, we used scanning electron microscope (SEM) to observe the microstructure of specimens with different fiber contents, and our results show that the gripping effect and binding effect are the main mechanisms of fiber reinforcement.

Key words: basalt fiber-reinforced silty clay; shear behavior; dynamic modulus; damping ratio; optimum fiber content

Cite this article as: JIA Yu, ZHANG Jia-sheng, WANG Xuan, DING Yu, CHEN Xiao-bin, LIU Tao. Experimental study on mechanical properties of basalt fiber-reinforced silty clay [J]. Journal of Central South University, 2022, 29(6): 1945−1956. DOI: https://doi.org/10.1007/s11771-022-5056-z.

1 Introduction

As an effective soil improvement technology, reinforcement has been widely applied in many projects, such as slopes [1], retaining walls, dams [2], highways, and railway subgrades [3]. In conventional reinforcement technology, continuous strips, sheet piles, or grid-like geotechnical materials are laid in the soil in a certain direction to

Foundation item: Project(51978674) supported by the National Natural Science Foundation of China; Project(2017G008-A) supported by the China Railway Corporation Science and the Technology Development Project
Received date: 2021-02-16; **Accepted date:** 2022-01-20
Corresponding author: DING Yu, PhD; Tel: +86-15315968071; E-mail: ding_yu0212@163.com; ORCID: https://orcid.org/0000-0002-8302-7326

improve the strength and stability of the soil. However, these reinforced materials laid in a certain direction tend to form potential fracture surfaces in the soil and increase the anisotropy of the soil [4−7]. The fiber reinforcement technology is to randomly distribute fibers in the soil, and can effectively solve the problem of soil anisotropy caused by conventional reinforcement technology [8 − 9]. More importantly, fiber reinforcement technology can significantly improve the shear strength [10−11], compressive and tensile strength [12−13], liquefaction resistance [14], and bearing capacity of the soil [12], reducing expansion [15−16] and dry-wet cycle cracking problems [17]. For these reasons, fiber reinforcement technology has been increasingly applied in geotechnical engineering.

Basalt fiber is a kind of environmentally friendly reinforced material and has the advantages of high strength, corrosion resistance, and high-temperature resistance [18]. In recent years, the mechanical properties of basalt fiber-reinforced soil have been widely studied. ZHENG et al [19] found that basalt fiber could improve the peak strength of tailings. RAMESH et al [20] studied the mechanical properties of basalt fiber-reinforced silt, and found that the basalt fibers with a length of 50 mm could improve the California bearing ratio (CBR) and unconfined compressive strength (UCS) of silt. GAO et al [21−22] conducted a UCS test on basalt fiber-reinforced clay and found that the UCS of basalt fiber-reinforced clay was significantly higher than that of pure clay. YOU et al [23] and XU et al [24] studied the influence of basalt fiber content on stress−strain curves of expansive soil and found that the optimum fiber content was approximately 0.4%. The research results of QU et al [25] also showed that basalt fiber can improve the shear strength of clay, and here the reinforcement effect was the best when the fiber content was 0.5%.

Most of the existing studies focus on the shear behavior of basalt fiber-reinforced soil, but studies on its dynamic characteristics are relatively lacking. As a soil improvement technology, basalt fiber-reinforcement has been increasingly applied in geotechnical engineering, especially in foundation reinforcement [26−28], and its dynamic characteristics should be further studied. In this paper, we conduct experimental research on shear behavior and dynamic parameter characteristics of basalt fiber-reinforced silty clay. We also use scanning electron microscope (SEM) to observe the microstructure of specimens with different fiber contents after triaxial tests to explore fiber reinforcement mechanism.

2 Materials and methods

2.1 Materials

2.1.1 Silty clay

The silty clay tested was taken from a construction site in Changsha, China. The undisturbed silty clay was tested for particle sieving according to the standard for geotechnical testing method (GB/T 50123—2019) [29], with the grain size distribution curve shown in Figure 1. In Figure 1, d_{10}, d_{30}, d_{50} and d_{60} are the grain sizes that correspond to the percentage finenesses of 10%, 30%, 50%, and 60%, respectively. The label C_u is the non-uniformity coefficient, and C_c is the curvature coefficient. Figure 1 shows that the silty clay is well graded.

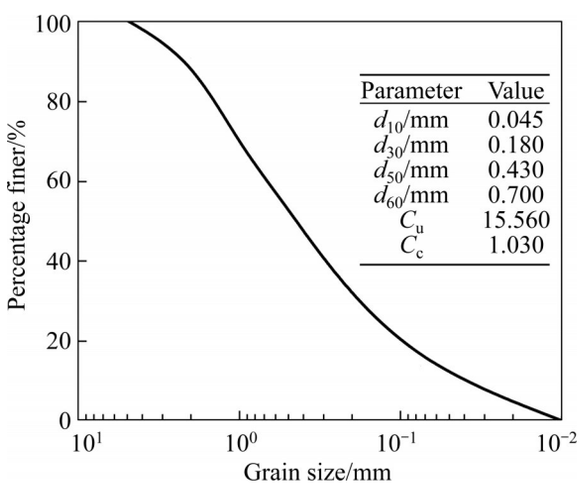

Figure 1 Grain size distribution curve for silty clay

The silty clay has a natural moisture content (ω) of 22.00%, a liquid limit (ω_L) of 30.76%, and a plastic limit (ω_P) of 16.53%. It has a liquid index (I_L) and plastic index (I_P) of 0.38 and 14.23, and is classified as a low liquid limit silty clay [29]. The maximum dry density (ρ_{dmax}) is 1.71 g/cm^3, and the optimum moisture content (ω_{opt}) is 18.50%.

2.1.2 Basalt fiber

The basalt fiber tested was obtained from a basalt fiber manufacturer in Jiangsu Province, China. The physical and mechanical parameters for the basalt fiber are listed in Table 1.

2.2 Test methods and programs

This paper analyzes the influence of basalt fiber content (FC=0%, 0.2%, 0.4% and 0.6%), moisture content (ω=16.0%, 18.5%, 20.0% and 22.0%), and confining pressure (σ_3=50 kPa, 100 kPa, and 150 kPa) on the shear behavior, dynamic modulus, and damping ratio of silty clay. The testing program is shown in Tables 2 and 3.

The monotonic triaxial test was carried out using the TSZ-1 strain-controlled triaxial apparatus, and the cyclic triaxial test used the DDS-70 microcomputer-controlled electromagnetic vibration triaxial test system. The test of SEM was performed with a JSM-IT500 scanning electron microscope. The monotonic and cyclic triaxial tests were performed in accordance with the standard for geotechnical testing method (GB/T 50123—2019) [29].

For our test we employed a remolded cylindrical specimen, with dimensions of 39.1 mm (diameter) and 80 mm (height). The specimen was prepared by the layered moist compaction and the under-compaction methods [30]. First, the silty clay was dried and crushed, and then the dry silty clay and fiber were mixed evenly according to the predetermined fiber content. And distilled water was added to the mixture according to the predetermined moisture content. After that, the wet soil was placed in a glassware for 24 h to ensure the uniform distribution of moisture. Then, the required quality

Table 1 Physical and mechanical parameters of basalt fiber

Density, ρ/(g·cm^{-3})	Length, L/mm	Monofilament diameter, D/μm	Tensile strength/MPa	Elastic model/GPa	Elongation at break/%
2.63–2.65	12	7–15	3000–4800	91–110	3.2

Note: The physical and mechanical parameters are provided by the manufacturer.

Table 2 Testing program for monotonic triaxial test

No.	Confining pressure, σ_3/kPa	Fiber content, FC/%	Moisture content, ω/%	Compactness/%	Shearing rate/(mm·s^{-1})
1	50	0	18.5	94	0.08
2	50	0.2	18.5	94	0.08
3	50	0.4	18.5	94	0.08
4	50	0.6	18.5	94	0.08
5	100	0	18.5	94	0.08
6	100	0.2	18.5	94	0.08
7	100	0.4	18.5	94	0.08
8	100	0.6	18.5	94	0.08
9	150	0	18.5	94	0.08
10	150	0.2	18.5	94	0.08
11	150	0.4	18.5	94	0.08
12	150	0.6	18.5	94	0.08
13	50	0.2	16.0	94	0.08
14	50	0.2	20.0	94	0.08
15	50	0.2	22.0	94	0.08
16	100	0.2	16.0	94	0.08
17	100	0.2	20.0	94	0.08
18	100	0.2	22.0	94	0.08
19	150	0.2	16.0	94	0.08
20	150	0.2	20.0	94	0.08
21	150	0.2	22.0	94	0.08

Table 3 Testing program for cyclic triaxial test

No.	Confining pressure, σ_3/kPa	Fiber content, *FC*/%	Moisture content, ω/%	Compactness/%	Loading waveform	Loading frequency/Hz
1	50	0.2	18.5	94	Sinusoidal	1
2	100	0	18.5	94	Sinusoidal	1
3	100	0.2	18.5	94	Sinusoidal	1
4	100	0.4	18.5	94	Sinusoidal	1
5	100	0.6	18.5	94	Sinusoidal	1
6	150	0.2	18.5	94	Sinusoidal	1
7	100	0.2	16.0	94	Sinusoidal	1
8	100	0.2	20.0	94	Sinusoidal	1
9	100	0.2	22.0	94	Sinusoidal	1

of soil for one specimen was calculated according to the density of the silty clay, fiber content and other parameters. The soil was divided into five layers and compacted. Before compaction of the next layer, the surface of the compacted layer was shaved to ensure good contact. Three specimens were prepared for each test program, and the average value of the three test results was calculated and recorded.

After the specimen preparation was completed, the specimen was installed in the triaxial cell for isotropic consolidation under the required confining pressure. After completion of consolidation, the monotonic triaxial and cyclic triaxial tests were carried out. For the monotonic triaxial test, the shear rate was 0.08 mm/s, and the test was ended when the shear strain reached 20% [29]. For the cyclic triaxial test, a staged loading method was adopted [29, 31]. The loading waveform was sinusoidal with a frequency of 1 Hz to simulate a train load or subway load [32−35]. The load amplitude of each stage was $0.1\sigma_3$, $0.2\sigma_3$ and $0.3\sigma_3$ (as shown in Figure 2), and the test was ended when the strain waveform showed obvious divergence [36]. Each stage was loaded 10 times, and the valve was opened to drain water and eliminate the influence of pore water pressure after the previous staged loading was completed. After these tests, specimens with different fiber contents were selected in order to observe the distribution characteristics of fibers in soil and to examine the microscopic mechanism of fiber reinforcement with scanning electron microscope.

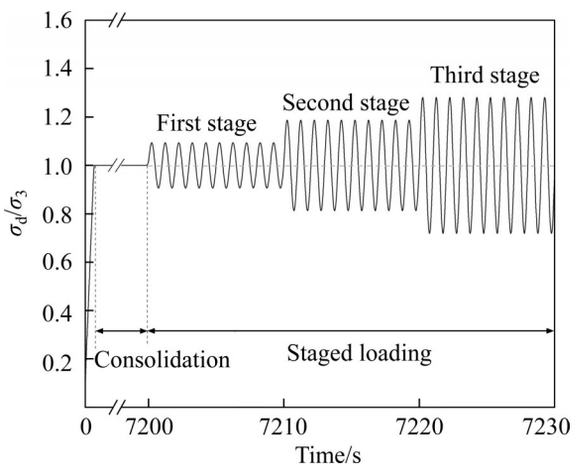

Figure 2 Diagram of staged loading

3 Test results and analysis

3.1 Shear behavior

3.1.1 Deviatoric stress−strain curves

Figure 3 shows the deviatoric stress (q)−strain (ε_a) curves for silty clay and fiber-reinforced silty clay. From Figure 3(a), we can see that the deviatoric stress increases with a increase in strain and shows a strain hardening characteristics. According to the standard for geotechnical testing method (GB/T 50123—2019) [29], the shear strength (q_f) is designated as the peak deviatoric stress or the deviatoric stress for ε_a=15% when there is no obvious peak deviatoric stress. q_f of the fiber-reinforced silty clay is greater than that of silty clay, indicating that the addition of fiber can significantly improve the shear strength of silty clay, and the shear strength of fiber-reinforced silty clay reaches its maximum when *FC*=0.2%.

The above analysis states that when *FC*=0.2%,

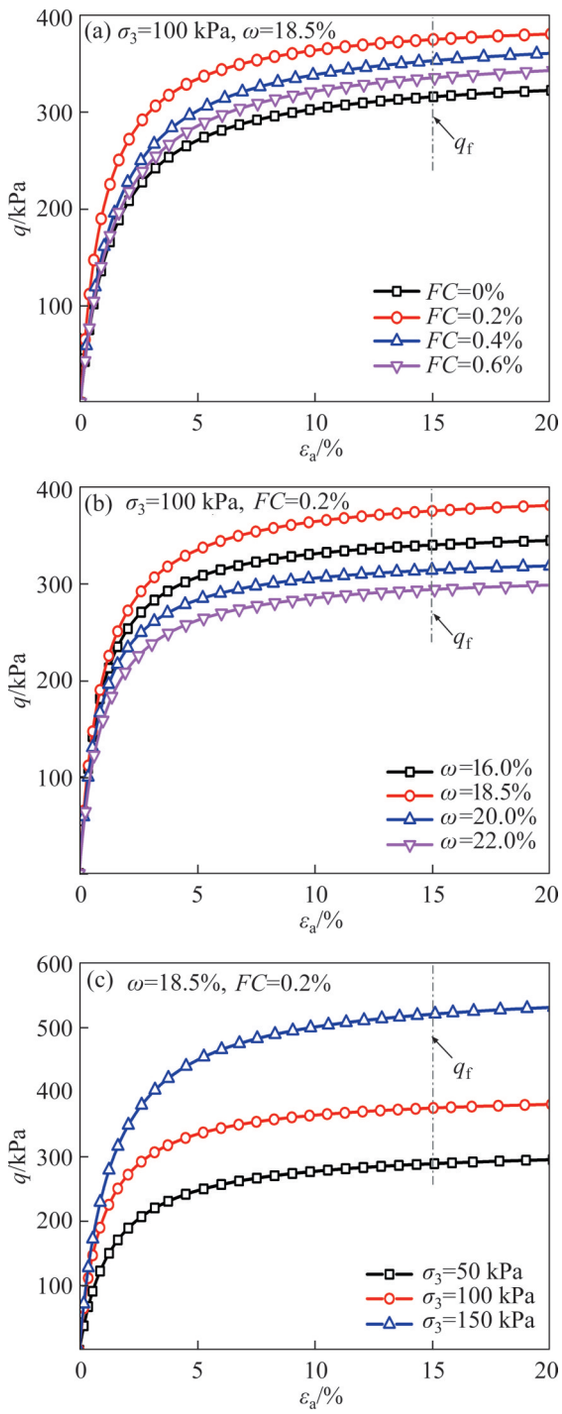

Figure 3 $q-\varepsilon_a$ curves: (a) Influence of fiber content; (b) Influence of moisture content; (c) Influence of confining pressure

the fiber-reinforced silty clay shows the best shearing behavior. Thus, we now further study the influence of the moisture content for fiber-reinforced silty clay with a 0.2% fiber content, as shown in Figure 3(b). The shear strength of fiber-reinforced silty clay first increases and then decreases as the moisture content increases. At the optimum moisture content of 18.5%, the shear strength of fiber-reinforced silty clay reaches its maximum; as the moisture content continues to increase, the shear strength decreases significantly.

Figure 3(c) shows the influence of the confining pressure on $q-\varepsilon_a$ curves of fiber-reinforced silty clay. Here we can see that the shear strength is positively correlated with the confining pressure because the specimen tends to form a denser state with a greater consolidation confining pressure and shows a higher shear strength.

3.1.2 Shear strength parameters c and φ

We used the Mohr-Coulomb criterion to describe the shear strength characteristics of silty clay and fiber-reinforced silty clay. From the $q-\varepsilon_a$ curves, we obtained the shear strength of each specimen under different confining pressures, and then the shear strength parameters (cohesion c and internal friction angle φ) were determined by linear regression analysis. Figure 4(a) shows the influence of fiber content on the cohesion and internal friction

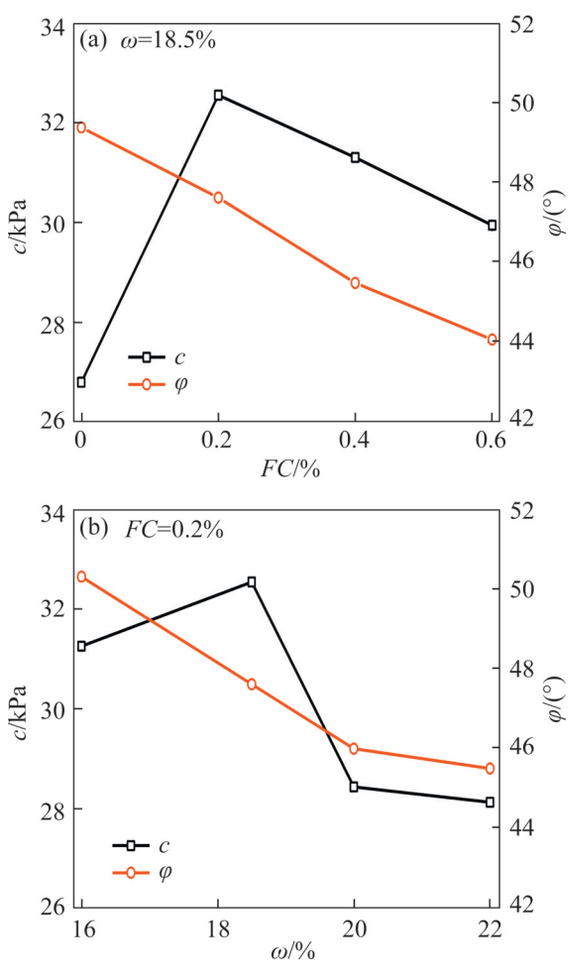

Figure 4 Shear strength parameters: (a) Influence of fiber content; (b) Influence of moisture content

angle. Here we see that the cohesion first increases and then decreases with increasing fiber content, and when FC=0.2%, the cohesion is the largest. As the fiber content increases, the internal friction angle decreases.

Figure 4(b) indicates that when the moisture content increases from 16% to 18.5% (the optimum moisture content), the cohesion increases to its maximum. With a continuous increase in the moisture content up to 20%, the cohesion decreases greatly. After this point, however, the cohesion decreases slightly with a continuous increase in the moisture content to 22%. Additionally, the internal friction angle decreases as the moisture content increases.

3.1.3 Analysis of the reinforcement effect

To analyze the reinforcement effect of basalt fiber further, we introduce the concept of the strength ratio (R) [4, 9], as shown in Eq. (1):

$$R = \frac{(q_f)_r}{(q_f)_u} \tag{1}$$

where $(q_f)_r$ is the shear strength of fiber-reinforced silty clay, and $(q_f)_u$ is the shear strength of unreinforced silty clay.

Figure 5 shows the strength ratios of fiber-reinforced silty clay with different fiber contents. The results show that the strength ratios for fiber-reinforced silty clay are all greater than 1.0, which again shows that the addition of fiber can increase the shear strength of silty clay. The strength ratio for silty clay with a fiber content of 0.2% is significantly higher than that of other contents,

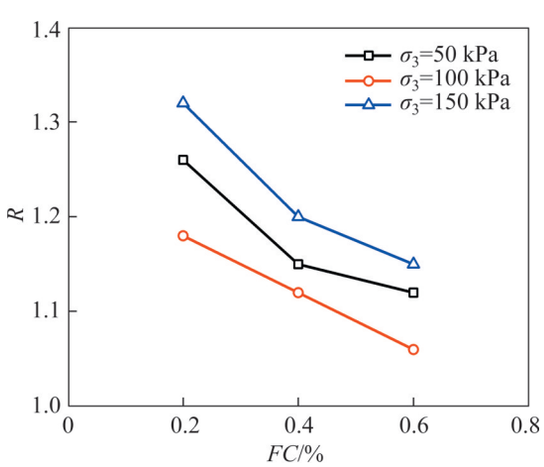

Figure 5 Strength ratios of fiber-reinforced silty clay with different fiber contents

which indicates that the reinforcement effect is the most obvious when the fiber content is 0.2%.

3.2 Dynamic modulus

3.2.1 Dynamic modulus–strain curves

Figure 6 shows the hysteresis curves (dynamic stress (σ_d) – strain (ε_d) curves) for cycle number N=32, 52, 72 and 92 for specimens with a fiber content of 0.2%, confining pressure of 150 kPa, and moisture content of 18.5%. The results show that the hysteresis curve of fiber-reinforced silty clay has the shape of an unclosed long shuttle. The unclosed hysteresis curve indicates that the strain cannot be completely recovered during the unloading process. That is, accumulative plastic strain is constantly produced during loading. In addition, with the increase in cycle number, the long axis of the hysteresis curve deflects to horizontal direction gradually, and the area of the hysteresis curve increases, which indicates the degradation of soil stiffness and increase in soil energy dissipation.

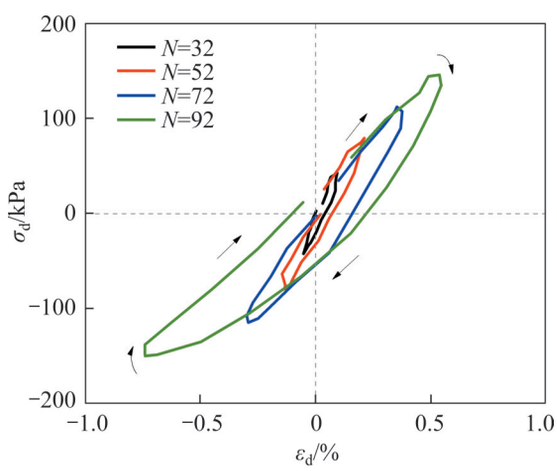

Figure 6 Hysteresis curves of fiber-reinforced silty clay for different cycle numbers

When we calculate the dynamic modulus and damping ratio, the unclosed dynamic stress (σ_d) – strain (ε_d) curve is artificially connected from end to end to form a closed hysteresis curve [35, 37], as shown in Figure 7, and the dynamic modulus is defined as [29]:

$$E_d = \frac{\sigma_{d1} - \sigma_{d2}}{\varepsilon_{d1} - \varepsilon_{d2}} \tag{2}$$

where E_d is the dynamic modulus; σ_{d1} and σ_{d2} are the maximum and minimum dynamic stresses in the hysteresis curve, respectively; ε_{d1} and ε_{d2} are the

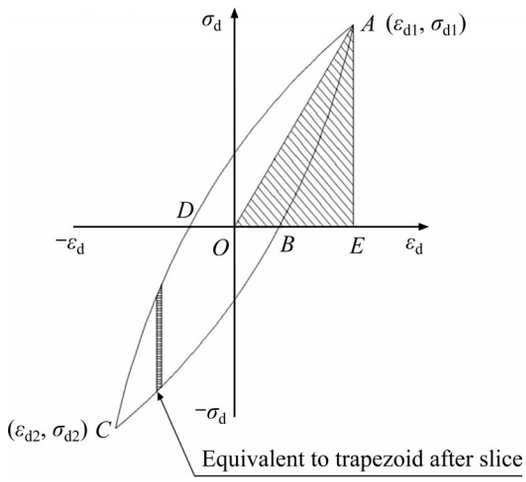

Figure 7 Schematic of a typical hysteresis curve [29]

maximum and minimum strains in the hysteresis curve, respectively.

Figure 8 shows the $E_d-\varepsilon_d$ curves for silty clay and fiber-reinforced silty clay. From Figure 8, we can see that when $\varepsilon_d \leqslant 0.1\%$, the E_d decreases linearly and rapidly with ε_d; when ε_d is in the range of 0.1%–1.0%, the E_d decreases nonlinearly with ε_d; and when $\varepsilon_d \geqslant 1.0\%$, the dynamic modulus tends toward a stable value. With increasing fiber content, the E_d for a given strain increases first and reaches its maximum when FC=0.2% and then decreases, and the E_d of fiber-reinforced silty clay is higher than that of unreinforced silty clay. Furthermore, as moisture content increases, the E_d first increases and then decreases, and the E_d of fiber-reinforced silty clay reaches its maximum when moisture content is 18.5%. Finally, we see that the E_d increases as the confining pressure increases.

3.2.2 Normalized dynamic modulus degradation curves

In 1972, HARDIN et al [38] proposed the relationship to determine the E_d of soil, as shown in Eq. (3):

$$E_d = \frac{1}{1+\dfrac{\varepsilon_d}{\varepsilon_r}} E_0 \tag{3}$$

where E_0 is the initial dynamic modulus, and ε_r is the reference strain. We use Eq. (3) to fit the $E_d-\varepsilon_d$ curves to obtain the values of E_0 and ε_r, which are listed in Table 4.

E_d obtained in the test is normalized with E_0, and we obtain the normalized dynamic modulus

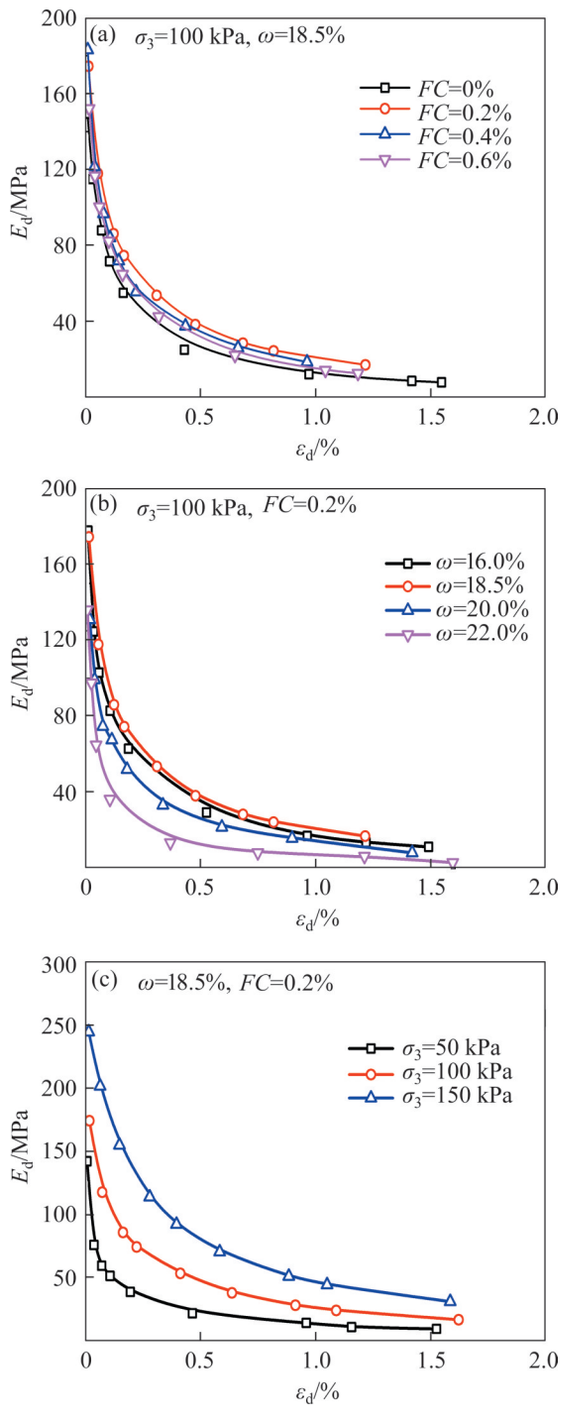

Figure 8 $E_d-\varepsilon_d$ curves: (a) Influence of fiber content; (b) Influence of moisture content; (c) Influence of confining pressure

degradation curves, as shown in Figure 9. The normalized dynamic modulus of silty clay and fiber-reinforced silty clay decreases with increasing strain, and they are all distributed in a band formed by two curves. The two degradation curves are the upper and lower boundary degradation curve, and the formulas for these curves are as follows.

Table 4 Values of E_0 and ε_r for Eq. (3)

No.	Confining pressure, σ_3/kPa	Fiber content, FC/%	Moisture content, ω/%	E_0/MPa	ε_r/%	R^2
1	100	0	18.5	166.8	0.078	0.99
2	50	0.2	18.5	163.9	0.034	0.98
3	100	0.2	18.5	192.6	0.106	0.99
4	150	0.2	18.5	263.0	0.161	0.99
5	100	0.4	18.5	202.4	0.077	0.98
6	100	0.6	18.5	177.7	0.089	0.98
7	100	0.2	16.0	194.8	0.076	0.99
8	100	0.2	20.0	152.4	0.086	0.97
9	100	0.2	22.0	170.7	0.031	0.99

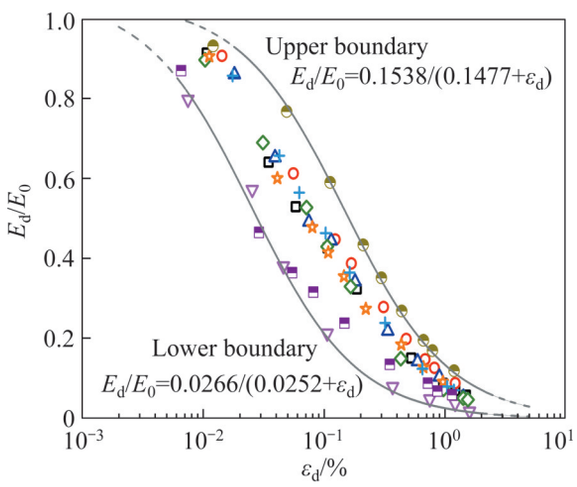

Figure 9 Normalized dynamic modulus degradation curves

$$\text{Upper boundary: } \frac{E_d}{E_0} = \frac{0.1538}{0.1477 + \varepsilon_d} \tag{4}$$

$$\text{Lower boundary: } \frac{E_d}{E_0} = \frac{0.0266}{0.0252 + \varepsilon_d} \tag{5}$$

3.3 Damping ratio

3.3.1 Damping ratio−strain curves

The damping ratio λ is defined as [29]:

$$\lambda = \frac{1}{4\pi} \times \frac{A}{A_S} \tag{6}$$

where A is the area of the hysteresis curve, as shown in Figure 7, and A_S is the area of the shaded part (the triangle ΔOAE) in Figure 7. The area of the hysteresis curve (A) is calculated by the slice method. That is, the hysteresis curve is divided into several vertical slices, and the area of each slice is calculated according to the area of the resulting trapezoid.

Figure 10 shows the damping ratio (λ) − strain (ε_d) curves for silty clay and fiber-reinforced silty clay. The damping ratio shows a nonlinear increase with increasing strain: when $\varepsilon_d \leqslant 0.1\%$, λ increases linearly; when ε_d is greater than 0.1% and less than 0.5%, λ increases nonlinearly; and when $\varepsilon_d \geqslant 0.5\%$, λ remains stable. Additionally, Figure 10(a) shows the effect of fiber content on the λ−ε_d curves. The results show that as the fiber content increases, the λ for a given strain first decreases and then increases. The maximum damping ratio for fiber-reinforced silty clay with FC=0.2% is approximately 12% less than that of unreinforced silty clay. Figure 10(b) shows the effect of the moisture content on the λ−ε_d curves. As the moisture content increases, λ first decreases and then increases. Figure 10(c) shows the effect of confining pressure on the $\lambda - \varepsilon_d$ curves. λ gradually decreases as the confining pressure increases since the contact between the fiber and the soil becomes denser with higher confining pressure, which leads to a decrease in the energy dissipation for fiber-reinforced silty clay.

3.3.2 Normalized damping ratio curves

The relationship between λ and ε_d presented in Figure 10 satisfies the following equation proposed by HARDIN et al [38]:

$$\lambda = \lambda_{max}\left(\frac{\varepsilon_d/\varepsilon_r}{1 + \varepsilon_d/\varepsilon_r}\right)^n \tag{7}$$

where λ_{max} is the maximum damping ratio, and n is a fitting parameter. We use Eq. (7) to fit the $\lambda - \varepsilon_d$ curves, and the values of λ_{max} and n are obtained as listed in Table 5. The coefficients of determination, R^2, are all greater than 0.90, indicating that Eq. (7) could accurately explain the damping ratio − strain curves of silty clay and fiber-reinforced silty clay.

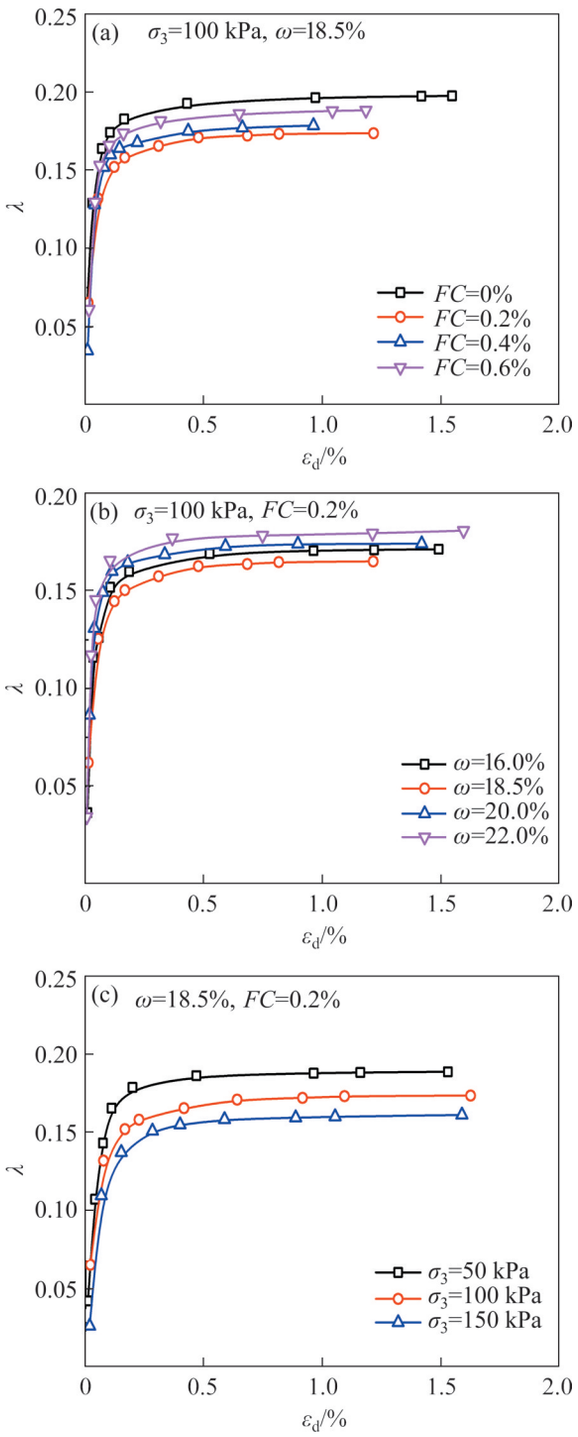

Figure 10 $\lambda-\varepsilon_d$ curves with effect of: (a) Fiber content; (b) Moisture content; (c) Confining pressure

Figure 11 shows the normalized damping ratio curves for silty clay and fiber-reinforced silty clay. The normalized damping ratio for silty clay and fiber-reinforced silty clay is concentrated in a narrow range. The fitting formulas for the upper boundary and lower boundary are shown in Eqs. (8) and (9), respectively.

Table 5 Values of λ_{max} and n

No.	Confining pressure, σ_3/kPa	Fiber content, FC/%	Moisture content, ω/%	λ_{max}/ MPa	ε_r/%	n	R^2
1	100	0	18.5	0.208	0.078	0.424	0.95
2	50	0.2	18.5	0.200	0.034	0.751	0.98
3	100	0.2	18.5	0.177	0.106	0.402	0.95
4	150	0.2	18.5	0.182	0.161	0.449	0.90
5	100	0.4	18.5	0.197	0.077	0.534	0.90
6	100	0.6	18.5	0.203	0.089	0.453	0.90
7	100	0.2	16.0	0.183	0.076	0.510	0.96
8	100	0.2	20.0	0.175	0.086	0.447	0.96
9	100	0.2	22.0	0.189	0.031	0.723	0.94

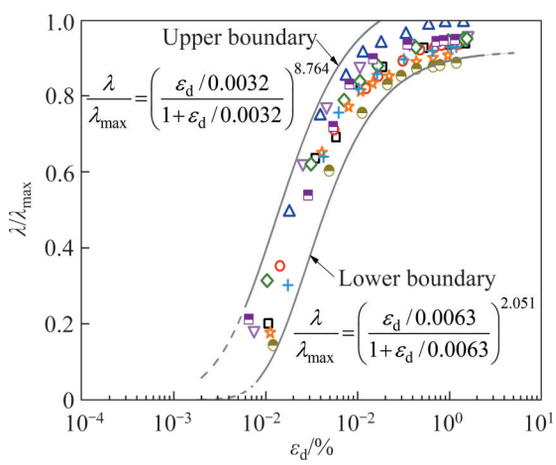

Figure 11 Normalized damping ratio curves

$$\text{Upper boundary: } \frac{\lambda}{\lambda_{max}}=\left(\frac{\varepsilon_d/0.0032}{1+\varepsilon_d/0.0032}\right)^{8.764} \tag{8}$$

$$\text{Lower boundary: } \frac{\lambda}{\lambda_{max}}=\left(\frac{\varepsilon_d/0.0063}{1+\varepsilon_d/0.0063}\right)^{2.051} \tag{9}$$

4 Discussion on fiber reinforcement mechanism

Figure 12 shows the SEM images of fiber-reinforced silty clay with FC=0.2%. Figure 12(a) indicates that a single fiber is tightly wrapped by surrounding clay particles, forming a gripping effect, which may enhance soil strength. Figure 12(b) indicates that fibers in some areas are interwoven to form a fiber network, and the binding effect of this fiber network may effectively restrain the surrounding soil particles and improve the soil strength.

Figure 13 shows the SEM image of fiber-

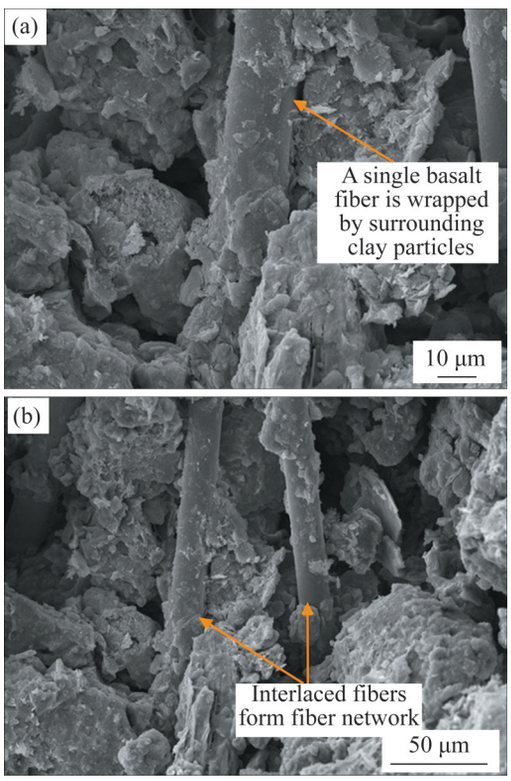

Figure 12 SEM images of fiber-reinforced silty clay with *FC*=0.2%: (a) Gripping effect between single fiber and soil; (b) Binding effect of fiber network

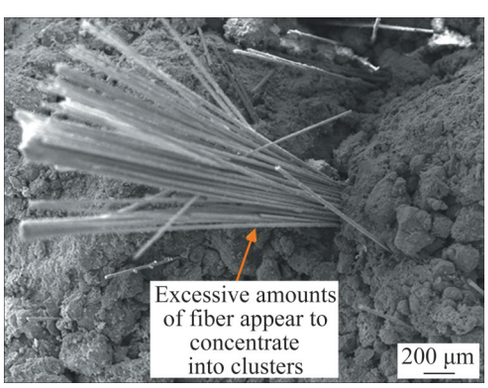

Figure 13 SEM image of fiber-reinforced silty clay with *FC*=0.6%

reinforced silty clay with *FC*=0.6%. Compared with Figure 12, we see that when the fiber content is 0.6%, the distribution of fibers in the soil becomes uneven, and some of fibers are concentrated into clusters. The clumped fibers have no direct contact with the soil particles, and the gripping effect between fibers and soil therefore may become weak. In fact, an excessive fiber concentration tends to form a weak structural surface in soil, resulting in a decrease in soil strength [39].

5 Conclusions

In this paper we studied the the shear behavior and dynamic parameter characteristics of basalt fiber-reinforced silty clay experimentally. The main conclusions are as follows.

1) The addition of basalt fiber can significantly improve the shear strength of silty clay especially when the fiber content is 0.2%, which is reflected in the increase in cohesion. The shear strength changes nonlinearly with a change in moisture content and is positively correlated with the confining pressure.

2) The dynamic modulus increases first and then decreases with the increase in fiber content and moisture content, and it increases as the confining pressure increases. However, the change in the damping ratio exhibits the opposite result. The upper and lower boundaries of the normalized dynamic modulus degradation curves and normalized damping ratio curves for fiber-reinforced silty clay are obtained.

3) By combining our analysis of the shear behavior and dynamic parameter characteristics of fiber-reinforced silty clay, we conclude that the optimum content of basalt fiber for use in silty clay is approximately 0.2%.

4) The microstructures of specimens with different fiber contents reveal what we characterize as a gripping effect between a single fiber and soil and a binding effect of the fiber network, which are the main mechanisms of fiber reinforcement.

Contributors

The overarching research goals were developed by ZHANG Jia-sheng, WANG Xuan, CHEN Xiao-bin, and LIU Tao. JIA Yu and DING Yu carried out the experiments and analyzed the data. CHEN Xiao-bin acquired the funding. The initial draft of the manuscript was written by JIA Yu, DING Yu, and WANG Xuan. All authors replied to reviewers' comments and revised the final version.

Conflict of interest

JIA Yu, ZHANG Jia-sheng, WANG Xuan, DING Yu, CHEN Xiao-bin, and LIU Tao declare that they have no conflict of interest.

References

[1] CHOU J S, NGO N T. Engineering strength of fiber-reinforced soil estimated by swarm intelligence optimized regression system [J]. Neural Computing and Applications, 2018, 30(7): 2129−2144. DOI: 10.1007/s00521-016-2739-0.

[2] KIM H J, WON M S, JAMIN J C. Finite-element analysis on the stability of geotextile tube − reinforced embankments under scouring [J]. International Journal of Geomechanics, 2015, 15(2): 06014019. DOI: 10.1061/(asce)gm.1943-5622.0000420.

[3] BORDOLOI S, HUSSAIN R, GARG A, et al. Infiltration characteristics of natural fiber reinforced soil [J]. Transportation Geotechnics, 2017, 12: 37−44. DOI: 10.1016/j.trgeo.2017.08.007.

[4] WANG Yi-xian, GUO Pan-pan, REN Wei-xin, et al. Laboratory investigation on strength characteristics of expansive soil treated with jute fiber reinforcement [J]. International Journal of Geomechanics, 2017, 17(11): 04017101. DOI: 10.1061/(asce)gm.1943-5622.0000998.

[5] ESTABRAGH A R, BORDBAR A T, JAVADI A A. Mechanical behavior of a clay soil reinforced with nylon fibers [J]. Geotechnical and Geological Engineering, 2011, 29(5): 899−908. DOI: 10.1007/s10706-011-9427-8.

[6] CHAKRABORTY T K D S. Randomly reinforced fly ash as foundation material [C]// Proceedings of the Indian Geotechnical Conference IGC96. Madras, India, 1996.

[7] GRAY D H A M. Admixture stabilization of sands with discrete, randomly distributed fibers [C]// Proceedings of XIIth International Conference on Soil Mechanics and Foundation Engineering. Rotterdam, Netherlands, 1989.

[8] SHARMA V, VINAYAK H K, MARWAHA B M. Enhancing compressive strength of soil using natural fibers [J]. Construction and Building Materials, 2015, 93: 943 − 949. DOI: 10.1016/j.conbuildmat.2015.05.065.

[9] PRABAKAR J, SRIDHAR R S. Effect of random inclusion of sisal fibre on strength behaviour of soil [J]. Construction and Building Materials, 2002, 16(2): 123−131. DOI: 10.1016/S0950-0618(02)00008-9.

[10] LIAN Bao-qin, PENG Jian-bing, ZHAN Hong-bin, et al. Effect of randomly distributed fibre on triaxial shear behavior of loess [J]. Bulletin of Engineering Geology and the Environment, 2020, 79(3): 1555 − 1563. DOI: 10.1007/s10064-019-01666-0.

[11] BOTERO E, OSSA A, SHERWELL G, et al. Stress-strain behavior of a silty soil reinforced with polyethylene terephthalate (PET) [J]. Geotextiles and Geomembranes, 2015, 43(4): 363 − 369. DOI: 10.1016/j.geotexmem.2015.04.003.

[12] TAN T, HUAT B B K, ANGGRAINI V, et al. Strength behavior of fly ash-stabilized soil reinforced with coir fibers in alkaline environment [J]. Journal of Natural Fibers, 2021, 18(11): 1556−1569. DOI: 10.1080/15440478.2019.1691701.

[13] ABDELDJOUAD L, ASADI A, BALL R J, et al. Application of alkali-activated palm oil fuel ash reinforced with glass fibers in soil stabilization [J]. Soils and Foundations, 2019, 59(5): 1552−1561. DOI: 10.1016/j.sandf.2019.07.008.

[14] KARAKAN E, ESKIŞAR T, ALTUN S. The liquefaction behavior of poorly graded sands reinforced with fibers [J]. Advances in Civil Engineering, 2018: 4738628. DOI: 10.1155/2018/4738628.

[15] ZHANG Dan, XU Qiang, GUO Ying. Experiments on strength and shrinkage of expansive soil with basalt fiber reinforcement [J]. Journal of Southeast University (Natural Science Edition), 2012, 42(5): 975−980. (in Chinese)

[16] LEI Sheng-you, DING Wan-tao. Experimental investigation on restraining the swell of expansive soil with fibre-reinforcement [J]. Chinese Journal of Geotechnical Engineering, 2005, 27(4): 482−485. (in Chinese)

[17] HAN Chun-peng, TIAN Jia-yi, ZHANG Jian, et al. Analysis of crack characteristics of fiber-reinforced expansive soil under wetting-drying cycle [J]. Journal of Jilin University (Engineering and Technology Edition), 2019, 49(2): 392 − 400. DOI: 10.13229/j.cnki.jdxbgxb20180019. (in Chinese)

[18] WANG Guang-jian, GUO Ya-jie, XU Ming-xia. Studies on filtration performance for ecocomposite of basalt fibers [J]. Journal of Functional Materials, 2009, 40(1): 130 − 134. (in Chinese)

[19] ZHENG Bin-bin, ZHANG Dong-ming, LIU Wei-sha, et al. Use of basalt fiber-reinforced tailings for improving the stability of tailings dam [J]. Materials (Basel, Switzerland), 2019, 12(8): 1306. DOI: 10.3390/ma12081306.

[20] RAMESH A, NAGESHWAR RAO C, KUMAR M. Experimental study on geocell and of fibre reinforced soil sub-grade under static and repetitive load [C]// Geotechnics for Transportation Infrastructure. 2019: 139 − 149. DOI: 10.1007/978-981-13-6713-7_11.

[21] GAO Lei, HU Guo-hui, CHEN Yong-hui, et al. Triaxial tests clay reinforced by basalt fiber [J]. Chinese Journal of Geotechnical Engineering, 2017, 39(S1): 198 − 203. (in Chinese)

[22] GAO Lei, HU Guo-hui, XU Nan, et al. Experimental study on unconfined compressive strength of basalt fiber reinforced clay soil [J]. Advances in Materials Science and Engineering, 2015: 561293. DOI: 10.1155/2015/561293.

[23] YOU Bo, XU Hong-zhong, DONG Jin-mei. Triaxial tests of expansive soil reinforced with basalt fibe [J]. Journal of Disaster Prevention and Mitigation Engineering, 2015, 35(4): 503−507, 514. DOI: 10.13409/j.cnki.jdpme.2015.04.015. (in Chinese)

[24] XU Hong-zhong, PENG Yi-qun, ZHAO Zhi-peng, et al. Experimental study on short basalt fiber reinforced expansive soil [J]. Building Science, 2012, 28(9): 44 − 47. DOI: 10.13614/j.cnki.11-1962/tu.2012.09.016. (in Chinese)

[25] QU Ji-li, HU Chen-kai, ZHAO Chao-nan. Shear strength experimental study on basalt fiber and nano slilca reinforced Shanghai clay [J]. Journal of Water Resources and Water Engineering, 2017, 28(3): 186−192. (in Chinese)

[26] DIAMBRA A, IBRAIM E, RUSSELL A R, et al. Modelling the undrained response of fibre reinforced sands [J]. Soils and Foundations, 2011, 51(4): 625 − 636. DOI: 10.3208/sandf.51.625.

[27] DIAMBRA A, IBRAIM E, WOOD D M, et al. Fibre reinforced sands: Experiments and modelling [J]. Geotextiles and Geomembranes, 2010, 28(3): 238 − 250. DOI: 10.1016/j.geotexmem.2009.09.010.

[28] SHARMA V, KUMAR A. Influence of relative density of

soil on performance of fiber-reinforced soil foundations [J]. Geotextiles and Geomembranes, 2017, 45(5): 499−507. DOI: 10.1016/j.geotexmem.2017.06.004.
[29] GB/T50123—2019. Standard for geotechnical testing method [S]. (in Chinese)
[30] SELIG E T, LADD R S. Preparing test specimens using undercompaction [J]. Geotechnical Testing Journal, 1978, 1(1): 16. DOI: 10.1520/gtj10364j.
[31] ZHAO Fu-tang, CHANG Li-jun, ZHANG Wu-yu. Experimental investigation of dynamic shear modulus and damping ratio of Qinghai-Tibet frozen silt under multi-stage cyclic loading [J]. Cold Regions Science and Technology, 2020, 170: 102938. DOI: 10.1016/j.coldregions.2019.102938.
[32] DING Yu, ZHANG Jia-sheng, CHEN Xiao-bin, et al. Experimental investigation on static and dynamic characteristics of granulated rubber-sand mixtures as a new railway subgrade filler [J]. Construction and Building Materials, 2021, 273: 121955. DOI: 10.1016/j.conbuildmat.2020.121955.
[33] BIAN Xue-cheng, JIANG Jian-qun, JIN Wan-feng, et al. Cyclic and postcyclic triaxial testing of ballast and subballast [J]. Journal of Materials in Civil Engineering, 2016, 28(7): 04016032. DOI: 10.1061/(asce)mt.1943-5533.0001523.
[34] YAN Chun-ling, ZHANG Ling, TANG Yi-qun. Microscopic experimental analysis of the accumulated plastic strain on a silty soil around a tunnel under a subway loading [J]. Geotechnical and Geological Engineering, 2020, 38(4): 3435−3447. DOI: 10.1007/s10706-020-01224-6.
[35] WEI Xin-jiang, ZHUANG Jia-huang, DING Zhi, et al. Research on the characteristics of hysteretic curves and damping ratio of frozen-thawed soils under cyclic subway loading [J]. Chinese Journal of Rock Mechanics and Engineering, 2019(10): 2092−2102. (in Chinese)
[36] HUANG Chang-xi, WANG Xing-hua, ZHOU Hao, et al. Dynamic elastic modulus and damping ratio of unsaturated red clay [J]. Geotechnical and Geological Engineering, 2020, 38(1): 873−881. DOI: 10.1007/s10706-019-01117-3.
[37] LUO Fei, ZHAO Shu-ping, MA Wei, et al. Quantitative research on morphological characteristics of hysteretic curves of Qinghai-Tibet frozen clay [J]. Chinese Journal of Rock Mechanics and Engineering, 2013, 32(1): 208−215. (in Chinese)
[38] HARDIN B O, DRNEVICH V P. Shear modulus and damping in soils: Design equations and curves [J]. Journal of the Soil Mechanics and Foundations Division, 1972, 98(7): 667−692. DOI: 10.1061/jsfeaq.0001760.
[39] BAO Xiao-hua, HUANG Yu-jun, JIN Zhi-yang, et al. Experimental investigation on mechanical properties of clay soil reinforced with carbon fiber [J]. Construction and Building Materials, 2021, 280: 122517. DOI: 10.1016/j.conbuildmat.2021.122517.

(Edited by ZHENG Yu-tong)

中文导读

玄武岩纤维加筋粉质黏土力学特性的试验研究

摘要：纤维加筋技术可以显著改善土体的力学性能，在岩土工程领域得到广泛的应用。玄武岩纤维作为一种新型环保的加筋材料，其与土体的力学性能得到越来越多的关注。本文通过三轴压缩试验以及动三轴试验研究了纤维含量、含水率以及围压等因素对玄武岩纤维加筋粉质黏土剪切特性、动弹性模量以及阻尼比的影响。试验结果表明：玄武岩纤维可以通过提高黏聚力来提高粉质黏土的剪切强度，当纤维含量为0.2%、含水率为18.5%(最优含水率)时，纤维加筋粉质黏土的剪切强度最大。随着纤维含量以及含水率的增加，相同动应变对应的动弹性模量呈现先增大后减小的变化趋势，当土体的纤维含量为0.2%、含水率为18.5%时，其动弹性模量最大；动弹性模量与围压呈现正相关关系。土体阻尼比随着纤维含量以及含水率的增加先减小后增大，随着围压的增加而减小。综合分析表明，本文所采用的玄武岩纤维最优含量在0.2%左右。纤维加筋粉质黏土的扫描电镜(SEM)结果表明：单根纤维与土体间的握裹作用以及纤维网间的约束作用是加筋土强度增强的主要机理。

关键词：玄武岩纤维加筋粉质黏土；剪切行为；动弹性模量；阻尼比；最优纤维含量